Uncovering the Structure of Heterogeneous Catalysts Using Atomic Pair Distribution Function Analysis

Nora K Zimmerli[a], Christoph R Müller[a*], and Paula M Abdala[a*]

[a] ETH Zürich, Department of Mechanical and Process Engineering, CH 8092 Zürich, Switzerland

*Correspondence: abdalap@ethz.ch (P.M. Abdala), muelchri@ethz.ch (C.R. Müller)

Keywords: Pair Distribution Function, Total scattering, Heterogeneous catalysis

Highlights

PDF analysis has become an important tool for the characterization of heterogeneous catalysts due to its ability to provide structural information across different length scales (local atomic environment to long-range structure).

As opposed to conventional diffraction methods, PDF does not require long-range order, making it ideal for the study of catalysts consisting of disordered phases, including defect-rich small nanoparticles or amorphous phases. Disorder in the PDF is visualized as deviations of the local from the average structure, making it a powerful tool to study crystal defects.

As heterogeneous catalysts are complex (multicomponent, multiphasic) materials, a difference PDF approach allows to identify contributions from different phases.

Abstract

Heterogeneous catalysts are complex materials, often containing multiple atomic species and phases with various degrees of structural order. The identification of structure – performance relationships that rely on the availability of advanced structural characterization tools, is key for a rational catalyst design. Structural descriptors in catalysts can be defined over different length scales from several Å up to several nanometers (crystalline structure), requiring structural characterization techniques covering these different length scales. Pair distribution function (PDF) analysis is a powerful method to extract structural information spanning from the atomic to the nanoscale under in situ or operando conditions. We discuss recent advances using PDF to provide insight into the atomic-to-nanoscale structure of heterogeneous catalysts.

PDF - a valuable technique to characterize the atomic structure of heterogeneous catalysts

Catalysis, being at the core of today's (petro)chemical industries, will be pivotal for our transition to more sustainable economies. Heterogeneous catalysts are typically complex materials containing different elements and phases with structures covering different length scales that often also dynamically change under reaction conditions. Revealing the detailed atomic structure, particularly at working conditions, is key for the rational advancement of novel and efficient catalysts [1]. This requires advanced tools that allow the characterization of a catalyst's structure across scales. While diffraction techniques are used to describe the crystalline phases of a material, they fail to describe complex catalyst systems with diluted active phases and in the absence of lacking long-range order. Local probes, such as extended X-ray absorption fine structure (EXAFS) [2] and solid-state nuclear magnetic resonance (ss-NMR) spectroscopy [3] are well-established for heterogeneous catalysts, each with their advantages and limitations [4,5]. On the other hand, PDF analysis can bridge the gap between the length scales accessible to diffraction methods (> ca. 3 nm [6]) and EXAFS (< 5-6 Å) [5]. The ability of PDF to probe structures at multiple length scales (~ from a few Å to several nm, the upper limit depending on the instrument [2]) makes it an ideal method to study the multiscale structures of catalysts, thereby complementing EXAFS and ss-NMR techniques.

The atomic pair distribution function (PDF) gives the probability of finding pairs of atoms separated by a distance *r*. Hence, this real space function provides direct insight into the short- and intermediate range order of materials at the nanoscale. The PDF can be derived experimentally from X-ray, (neutron or electron) total scattering patterns, or it can be calculated from a model structure [7]. **Total scattering** (see Glossary) includes contributions from both Bragg (coherent) and diffuse (non-coherent) scattering that are associated with periodic order and disorder, respectively [8]. Structural information arising from both contributions is contained in the PDF, making it a powerful method for the study of disordered and nanostructured materials that are frequently used as heterogeneous catalysts [9]. In recent years, advancements in instrumentation and data analysis have enabled PDF to become an increasingly valuable tool for the characterization of heterogeneous catalysts [10,11]. In combination with complementary spectroscopy techniques and theoretical calculations, PDF analysis has provided fundamental structural insights into heterogeneous catalysts [12–14].

Measuring total scattering data and analysing a PDF

For PDF analysis, we collect total scattering data optimized for a high maximum momentum transfer Q (magnitude of the momentum transfer vector $\boldsymbol{Q}$), defined by the scattering angle θ and the wavelength of the incident radiation λ:

$$Q = \frac{4\pi sin\theta}{\lambda} \quad [1]$$

Several corrections [15] are then applied to the measured scattering intensities $I(Q)$ to obtain the total structure function $S(Q)$, representing the normalized, coherently scattered signal intensity from the sample. For X-rays, it is defined as follows:

$$S\,(Q) = \frac{I_c(Q) - \langle f(Q)^2\rangle + \langle f(Q)\rangle^2}{\langle f(Q)\rangle^2} \quad [2]$$

where $\mathrm{I_c}(Q)$ is the coherent scattering intensity and $f(Q)$ are the atomic form factors of the elements in the sample [15]. Finally, a Fourier transform is applied to $S(Q)$ to obtain the PDF or $G(r)$ (Figure 1A):

$$G(r) = \left(\frac{2}{\pi}\right) \int_{Q\mathrm{min}}^{Q\mathrm{max}} Q(S(Q) - 1)\sin(Qr)\, dQ \quad [3]$$

The larger the probed Q-range, the more information can be extracted from the PDF. Typically, Q_{max} (the maximum Q measured) should be above 15 – 20 Å^{-1} to obtain structural information on the atomic scale with enough real space resolution.

PDF can be acquired from X-ray, electron or neutron scattering experiments. For X-rays, the atomic scattering power increases with the atomic number and consequently, X-ray PDF is more sensitive to heavy elements than to lighter ones. Light atoms such as H, C or O interact strongly with neutrons, making neutron PDF the preferred approach [16]. High energy electrons interact more strongly with matter than X-rays and neutrons and are widely available in transmission electron microscopes (TEMs) with high incident energies (80-300 kV, resulting in high Q_{max}), allowing to study small areas of a sample with high spatial resolution. A limitation of electron PDF is that the absolute number of scattered electrons is low due to the small sample volumes probed, leading typically to poorer signal-to-noise ratios than for X-ray PDF. A variety of software is available to obtain $S(Q)$ and $G(r)$ from experimental total scattering data from X-rays, neutrons or electrons such as PDFgetX3 [17], PDFgetN3 [18], GSAS-II [19], Gudrun X and Gudrun N [20]. The obtained PDF can be analysed either without assuming any structural model to describe the data (model-free analysis) or by testing and

refining structural models against the PDF data (PDF modelling). A key advantage of real space analysis over conventional reciprocal-space powder diffraction analysis lies in the direct, model-free structural information obtained. In this context the following features of the PDF can be analysed (Figure 1B): i) Peak positions that correspond directly to interatomic distances within a material. ii) Peak areas that are proportional to the relative abundance of the atomic pair to which the peaks correspond to, and thus allow to determine coordination numbers from peak areas [21]. iii) Peak widths that represent a distribution of interatomic distances around the average peak position. Peak broadening is caused by positional disorder of atoms, e.g. due to atomic vibrations or static disorder [11]. iv) The maximum distance r_{max} above which no PDF features exist serves as an estimate for the domain size [22]. v) The slope of the PDF at low r gives an estimate of the atomic density [21]. In addition, when a time series of PDF data is available (such as from in situ studies), the monitoring of the above described PDF features over time allows for the determination of quantitative kinetics, changes in concentration or in the atomic structure without the need for a structural model [22]. A more comprehensive analysis can be obtained through PDF modelling [21]. Here, a model PDF calculated from either a discrete structural model (cluster of atoms larger than the range of the model PDF) or a crystal structure is fitted to the experimentally obtained PDF. These two different approaches to obtain a model PDF are referred to as big box and small box modelling, respectively, and should be chosen depending on the research question to be answered [21]. By comparison of the model and experimental PDF, a residual function can be derived to quantify the "goodness-of-fit". The goal of PDF modelling is to find a three-dimensional structure that represents best the data. This can be done e.g., by testing different models against an experimental PDF and refining their parameters within reasonable constraints by least-squares minimization. Widespread software for small box modelling include PDFGui, [23] TOPAS, [24] and DiffPy-CMI [25] whereas DISCUS [26], DiffPy-CMI, RMC++ [27] or RMCProfile [28] allow big box modelling.

Having introduced the basis of PDF, we will review now recent applications of PDF for the study of heterogeneous catalysts. Particular emphasis will be given to the study of catalyst structures across different length scales, spanning from small clusters of atoms to nm-sized particles or domains.

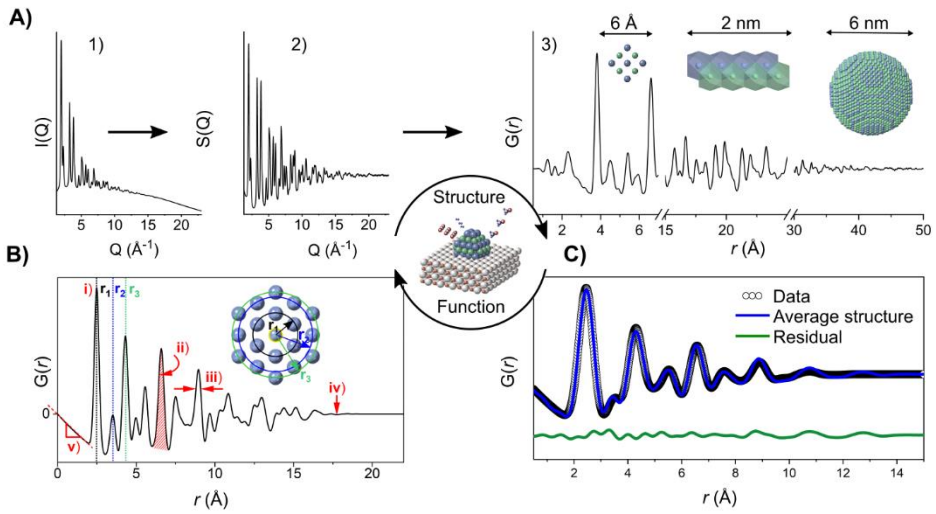

Figure 1. PDF data collection, processing and interpretation. *(A) Schematic procedure to obtain a PDF from total scattering data and the different ranges of structural order covered by PDF for the example of a nanoparticle (B) Key features of a PDF and the structural information contained within them: i) peak positions correspond to interatomic distances, ii) peak areas are proportional to coordination numbers, iii) peak widths relate to disorder, iv) the maximum r above which there are no more PDF peaks is an estimate of the ordered domain size and v) the initial slope of the PDF is related to the atomic density. Redrawn from [9]. (C) Exemplary PDF fitting, highlighting the ability of PDF to resolve local disorder as the mismatch between the experimentally obtained data (black curve) and an average structure model (blue curve).*

Crystal defects – the mismatch between the local and average structures

Catalysts often contain defects (such as vacancies, local distortions, staking faults, etc.) in their bulk and surface structures which can affect the material's catalytic performance [29]. However, to understand how defects in the crystal structure affect a particular reaction we require methods capable of probing the local and average structures.

For instance, nanostructured materials can exhibit a high density of defects as well as size-dependent phases, making PDF analysis instrumental to assess their structure in detail [14]. When a mismatch between the local and the average structure is found, it indicates structural disorder (Figure 1C). For instance, PDF analysis showed that the local structure (between 1 to 8 Å) of metastable γ-Ga_2O_3 nanocrystals with various applications in catalysis [30–32] deviates from the average cubic spinel-type structure due to a high degree of structural disorder [33]. The disorder arises from a distortion of the Ga-O polyhedra, which are randomly oriented

within the nanocrystal (Figure 2A). In situ time resolved (1 s) PDF revealed that the gradual transformation of the γ-Ga_2O_3 nanocrystals toward the thermodynamically stable β-Ga_2O_3 polymorph occurs at different temperatures and in different structural domains (Figure 2B). Particularly, at low temperature (ca. 300 °C) the appearance of subnanometric β-Ga_2O_3 domains was revealed, pointing out to the presence of γ/β-Ga_2O_3 much below the bulk transition temperature that can be observed by conventional XRD (600-750°C), which may have implications for their photo/thermal catalytic performance [33].

Oxygen vacancies in metal oxide catalysts may play an important role in governing their catalytic properties [29]. Using neutron PDF in combination with Raman spectroscopy, the oxygen vacancy arrangement in ceria nanorods and nanocubes was studied in-depth [34]. For both partially pre-reduced materials, Frenkel-type oxygen vacancies were dominant in the bulk structure whereas the surface was rich in an oxygen-deficient ceria phase with ordered oxygen vacancies ($Ce_3O_{(5+x)}$, Figure 2C). Also, nanorods had a larger concentration of surface oxygen defects than nanocubes. This was related to the different activation energies for oxygen vacancy formation on {110} and {100} facets (dominant for nanorods) compared to {100} facets (dominant for nanocubes), in line with density functional theory (DFT) calculations. Additionally, insight into the deactivation mechanism of ceria-based catalysts in three-way catalytic converters was obtained by tracking the evolution of the oxygen vacancy concentration during heating to 600°C in vacuum for pre-reduced and SO_2-treated nanorods and nanocubes. It was found that SO_2 has an inhibitive effect on surface and bulk oxygen vacancy formation as evidenced by their reduced concentration in the SO_2 treated samples compared to the as-reduced samples. Therefore, methods to stabilize surface oxygen defects in ceria catalysts would lead to materials with a more stable performance.

PDF has been also applied to unravel complex disorder in layered structures [16,35–42]. For example, δ-MnO_2 is a layered material which has attracted attention as catalyst for water splitting [43,44]. The catalytic properties of the δ-MnO_2 nanoparticles are strongly correlated with the specific types of the interlayering cations, yet the relationship between structure and function remains under investigation. The structural analysis of nm-sized δ-MnO_2 is highly challenging due to the presence of disorder that arises largely from: i) turbostratic stacking faults and ii) the interactions between interlayering cations and interlayering water molecules. The use of complementary neutron and X-ray PDF analyses in combination with X-ray absorption spectroscopy (XAS) allowed for the accurate description of the local-to-average structure of Cu-rich δ-MnO_2 [16]. Initially, the local structure was refined against X-ray based

PDF in the range of 0.8-8 Å using a chalcophanite-like supercell, allowing for the quantification of Mn^{4+} vacancies in the MO_2 layers and identification of the location of Cu^{2+} in the interlayer sites above and below the Mn vacancies. The model was further complemented by the interlayer water positions, which play a role in maintaining the layered structure, obtained from neutron PDF analysis. Next, the intermediate and long-range order structures were refined, incorporating a model of turbostratic stacking faults as well as the sheet-like morphology of the material. This approach established a methodology for PDF analysis to resolve the structure of disordered, layered materials on different length scales.

The studies described above open up future opportunities for the use of PDF analysis in combination with catalytic characterization, ideally simultaneously in an operando fashion, to understand how the defective structure of materials affects their performance.

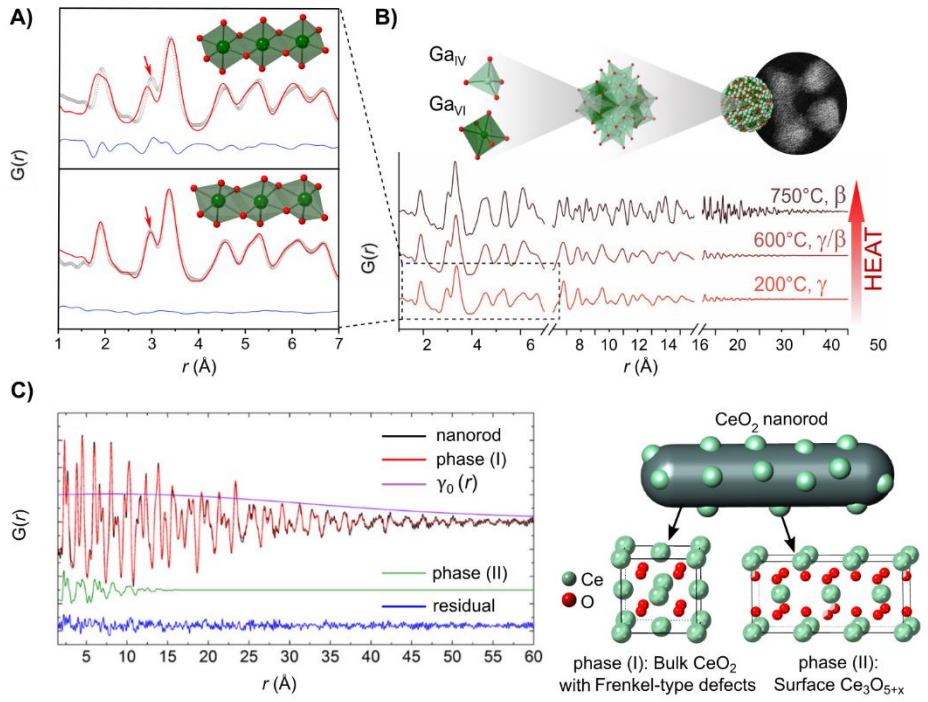

Figure 2. Defect-rich structures. *(A) Distorted (bottom) rather than symmetric (top) polyhedra, best describe the local structure of disordered γ-Ga_2O_3 nanoparticles. (B) Different structural domain transformations observed during the heat-induced phase transition from γ-Ga_2O_3 to β-Ga_2O_3. Adapted with permission from [33]. (C) PDF fitting of CeO_2 nanorods containing Frenkel-type oxygen vacancies in the bulk (phase I) and an oxygen deficient ceria phase with ordered oxygen vacancies (phase II) dispersed on the surface. Adapted with permission from [34].*

Finding local order in XRD-amorphous catalysts

Materials lacking long-range order do not display Bragg peaks in XRD patterns and are typically described as amorphous, yet they exhibit a distinctive local atomic arrangement that dictates their catalytic properties. PDF analysis has proven instrumental to characterize heterogeneous catalysts or pre-catalysts lacking long-range order [45–50]. Key structural motifs in IrO_x hydroxide catalysts for the oxygen evolution reaction (OER) were identified by an (electron microscopy based) ePDF study in combination with other electron microscopy techniques [51]. Two amorphous IrO_x materials that exhibit different electrocatalytic performance, were interrogated by ePDF analysis and it was shown that in one material the IrO_6 octahedra were connected predominantly via corners, with rutile-like domains, while in the other material the IrO_6 octahedra were connected in equal proportions via corners and edges, with hollandite-like domains (Figure 3A). Rutile-like domains correlated with poor catalytic performance, whereas a higher activity and stability were associated with hollandite-like structural domains. Synthetic control over the structure and arrangement of structural motifs in IrO_x hydroxides could thus allow to further improve the material's performance for catalytic water splitting.

Insight into the link between the local and electronic structure of two different amorphous iridium oxide based OER catalysts, viz. iridium blue layer (IrBL) and IrO_x, was obtained using X-ray PDF in combination with Ir L_{III} edge resonant inelastic X-ray scattering (RIXS) and DFT calculations [49]. The previously identified, edge- and corner-connected octahedral IrO_6 structural units also appeared in the local structure of the IrO_x and IrBL catalysts (Figure 3C). Compared to rutile IrO_2, both materials showed significant structural local distortions, similar to the trigonal distortion of TiO_6 octahedra found in Ti_2O_3. In IrO_x the distortion was more pronounced than in IrBL, which correlated with a higher electrical conductivity and a higher OER activity of IrO_x compared to IrBL (Figure 3B). In fact, the differences in atomic local structure between the two materials led to significant changes in the Ir 5d electronic structures, as revealed by Ir L_{III} RIXS and ab-initio calculations. Importantly, integer and non-integer filling of the Ir 5d bands observed in IrBL and IrO_x depict metallic and insulating ground states respectively, which explains the differences in their electrical conductivity and thus, OER activity.

Overall, these studies bring forward a methodology to decipher the intricate interplay between atomic and electronic structures in catalysts without a long-range order yet distinct local structure, resulting in materials with vastly different catalytic properties.

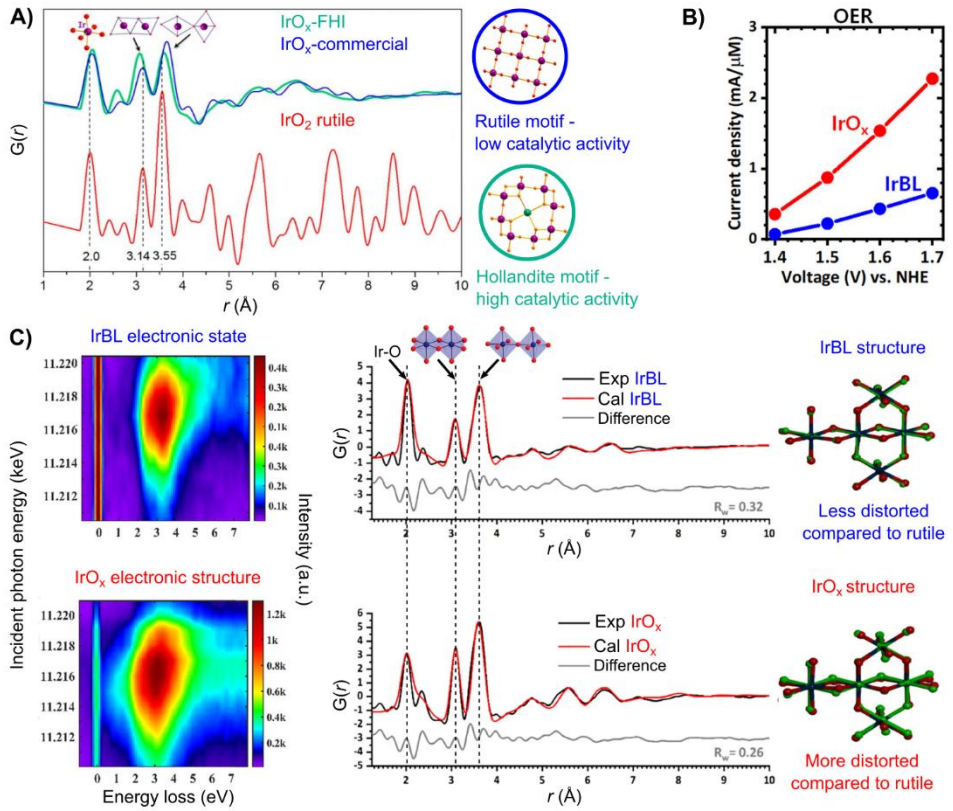

Figure 3. Amorphous catalysts*. (A) ePDF of two amorphous IrO_x based catalysts for the oxygen evolution reaction (OER) and rutile IrO_2. The hollandite structural motif found in IrO_x-FHI correlated with a high OER activity whereas the rutile motif in IrO_x-commercial was associated with a poor OER performance. Adapted with permission from [45]. (B) OER performance of two amorphous IrO_x based catalysts, IrO_x and IrBL. (C) RIXS patterns, PDF and obtained structure models of IrBL (top) and IrOx (bottom). Note that the structure models of IrOx and IrBL (green) are overlaid with the rutile IrO_2 structure (red) to visualize the greater distortion of IrO_x compared to IrBL which correlated with a higher OER activity. (B) and (C) adapted with permission from [49].*

PDF of supported nanoparticles catalysts - when differences matter

The active phase, or active site [1], which takes part in a catalytic reaction, typically consists of nm-sized particles, sub-nm sized clusters or single metal sites. The active phase can be dispersed on a material (support) with a large specific surface area to ensure high metal dispersion, to prevent agglomeration under operating conditions and sometimes to improve catalytic performance by the creation of interfacial sites [11]. The total PDF of such multicomponent materials is a linear combination of contributions from the active phase, the support material, and interactions between them. Due to the additive nature of these contributions, the pair correlations of the active phase and support interactions can be isolated by subtracting the PDF signal of the pristine support measured under equal conditions from the total PDF (Figure 4A). The resulting PDF can been referred to as difference (or differential)

PDF (d-PDF) [9]. This approach has been applied to a vast variety of supported catalysts [31,47,52–64] . For example, d-PDF analysis allowed to characterize in detail the supported phases in gallium oxide-based catalysts for propane dehydrogenation (PDH) [31]. The crystallite size, local and intermediate-range structure of nanocrystalline γ-Ga_2O_3 supported onto amorphous SiO_2 (γ-Ga_2O_3/SiO_2) was in stark contrast to the local structure of amorphous GaO_x supported on SiO_2 (GaO_x/SiO_2). These catalysts exhibited different activities and selectivities for propene as well as surface properties, allowing the derivation of structure performance relationships. The same approach can be applied when using crystalline supports. For example, using d-PDF and automated cluster fitting, the atomic structure of nanoscale MoO_x supported onto γ-Al_2O_3 was determined, which was described by a distribution of polymeric [MoO_x] clusters [65]. In a further study, d-PDF was used to isolate the pair correlations of a polyoxometalate (POM) and a photocatalytic Rh complex (Rh-cat.) immobilized in UiO-67 [60] (Figure 4C). In this case, d-PDF analysis allowed to confirm that the structure of these molecules was preserved after their co-immobilization in UiO-67 and after exposure to CO_2 reduction conditions (Figure 4B). d-PDF can also aid the elucidation of guest-host (support) interactions [60,61,64,66,67]. This was demonstrated e.g., for Cu-oxo species deposited via atomic layer deposition (ALD) in a Zr-based MOF (NU-1000) [68]. After ALD deposition of the Cu precursor, d-PDF analysis revealed newly formed M-Zr (M = Cu, Zr) and Cu-Zr pair correlations, indicating the location of the Cu-oxo species in the vicinity of the Zr nodes in NU-1000 (Figure 4D). A negative pair correlation at 3.57 Å was assigned to Zr-Zr in pristine NU-1000 which was the result of a structural distortion of the support during dehydration. This (negative) feature further intensified during a reductive treatment, simultaneous with the restructuring of the Cu precursor to Cu nanoparticles (ca. 4 nm) and sub-nm Cu^0 clusters. The studies summarized above make clear that d-PDF provides reliable data for the analysis of supported nanoparticles, yet a carful interpretation of the data is essential to distinguish between the nanoparticle's structure and interfacial sites.

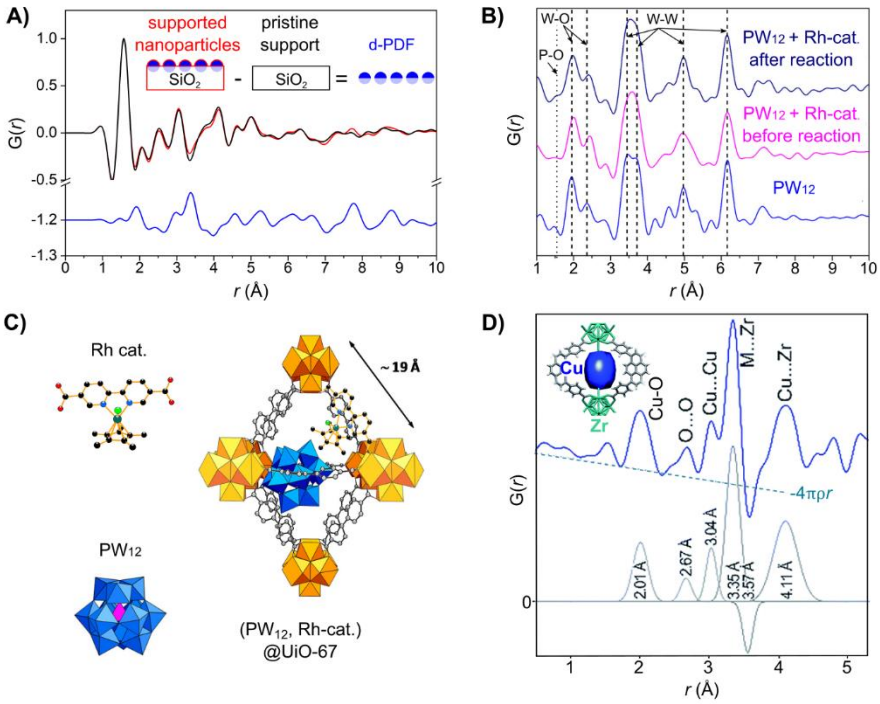

Figure 4. d-PDF analysis. *(A) Schematic concept of d-PDF using SiO_2 supported γ-Ga_2O_3 nanoparticles as an example. (B) d-PDF of a polyoxometalate (PW_6) and a Rh containing photocatalyst (Rh cat.) encapsulated in UiO-67 before and after photocatalytic CO_2 reduction. The d-PDF of PW_{12} encapsulated in UiO-67 is also shown as reference. (C) Schematic of the PW_{12} cluster and Rh cat., as well as their location within a pore of UiO-67. (B) and (C) adapted with permission from [60]. (D) d-PDF of Cu oxo clusters supported in NU-1000. The schematic shows the location of the Cu oxo clusters in the pores between the Zr_6 nodes of NU-1000. Adapted with permission from [68].*

Probing hierarchical structures and their evolution under reactive conditions

PDF has been exploited for the study of a variety of hierarchically structured materials, such as zeolites [69–71] and metal organic frameworks, MOFs [68,72,73] where local, Å-sized structural motifs (e.g. polyhedral metal oxide clusters) are interconnected to form Å-nm sized pores, potentially containing catalytically relevant guest species. SAPO-34 is a microporous zeolite catalyst widely used for the methanol to olefins process and the selective reduction of NO_x with NH_3 [74]. For both processes, SAPO-34 is pre-treated under hydrothermal conditions which has a significant effect on its structure as revealed by in situ ss-NMR and PDF [69]. When heated under steam, a sudden change in the Al-O bond lengths was observed by PDF (Figure 5A) which fell within the same temperature range (250-300°C) for which in situ ss-NMR showed changes in the local structure around the catalytically important Brønsted acidic

Si-O-H sites. These changes were attributed to the interaction of the Brønsted acid sites with water and highlight the importance of studying the structure of catalysts under relevant conditions by complementary PDF and spectroscopic techniques.

The well-defined, versatile hierarchical crystal structure of MOFs has been exploited to develop synthetic routes to produce supported nanoparticles of controlled sizes, phases and compositions [57,63,73]. In this context, MOFs have been proposed as precursors to produce well-dispersed metal centres supported onto carbon [57]. For example, the thermal degradation of PCN-250 MOF containing iron (Fe_3) and bimetallic (Fe_2Co, Fe_2Ni) nodes was followed via in situ PDF to understand the mechanism of (bi)metallic nanoparticle formation [73] (Figure 5B). Detailed and time resolved insight of the long- and short-range structure was revealed by PDF analysis. During heating under a reductive atmosphere, a threshold temperature was determined below which changes in the local structure of the nodes took place without loss of long-range order. Above the threshold temperature, the formation of nanoparticles, containing metallic and disordered oxide phases, started simultaneously with the loss of long-range order. Interestingly, the partial reduction of Ni^{2+} to Ni^0 or Fe^{3+} to Fe^{2+} in the MOF nodes took place below the threshold temperature, with the long-range order of the PCN-250 framework unchanged. The obtained insight may lead to new routes to modify the chemistry of MOFs via post-synthesis treatment to yield well-defined, model nanomaterials. Moreover, these studies demonstrate the importance of developing time resolved in situ / operando setups to fully utilize the capabilities of PDF analysis.

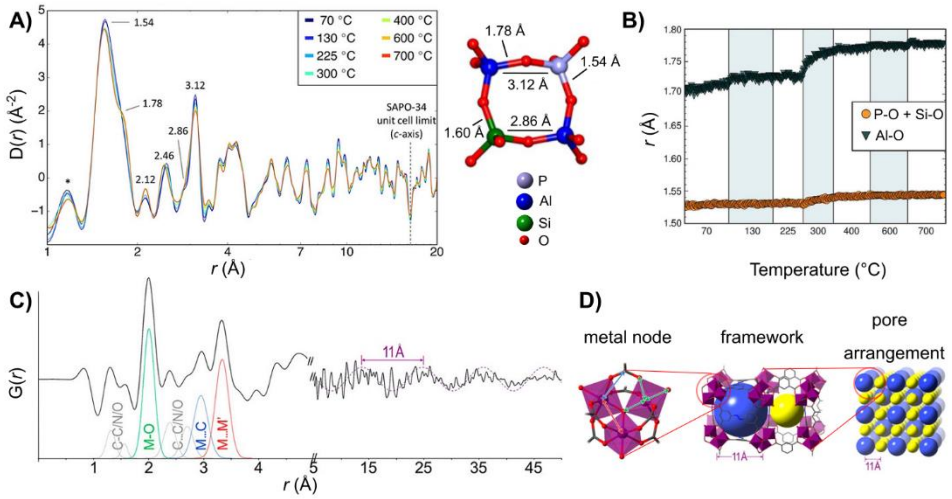

Figure 5. Hierarchical pore structures. *(A) In situ PDF of SAPO-34 during steam treatment at different temperatures. The labelled interatomic distances are indicated in the local structure model given on the right. (B) Evolution of the interatomic distances of (P-O, Si-O) and Al-O as a function of temperature. (A) and (B) adapted with permission from* [69]. *(C) PDF of a PCN-250 MOF with (bi)metallic nodes (M = Fe/Ni/Co). (D) Hierarchical structure of PCN-250. (C) and (D) adapted with permission from* [73].

Concluding Remarks and Future Perspectives

PDF analysis is a very powerful tool to resolve the atomic structure of heterogeneous catalysts at different length scales, viz. from the distance between neighbouring atoms up to several nanometers. We have illustrated through several examples, how PDF can be applied to elucidate the structure (and changes thereof) of different heterogeneous catalytic systems, viz. nanoparticles, layered structures, amorphous materials, and materials with a hierarchical porous structure. We believe that further improvements in instrumentation and data analysis will establish PDF as a versatile toolbox to study catalyst structures across scales (see Outstanding Questions). Pivotal questions in heterogeneous catalysis are, how does the structure of a catalyst correlate to its performance? And how does the structure change under reaction conditions? To answer these two questions for a particular system, the development of tailored in situ/operando setups to interrogate the structure of a catalyst under relevant reactive conditions is key [75–78]. Moreover, the design and construction of setups to allow the (quasi) simultaneous acquisition of X-ray total scattering data in combination with complementary spectroscopic techniques under reaction conditions, such as XAS, infrared, Raman or energy dispersive X-ray spectroscopies, would be highly valuable [70,79–81]. Such combined setups will provide the relevant data to formulate robust structure - performance

relationships as they avoid difficulties in reproducing identical conditions with different setups (for the respective individual techniques). In addition, we expect a rapid growth of PDF applications with recent advances in laboratory based X-ray PDF systems [46,82–85] as well as e-PDF [51,86–91]. Such developments will increase the accessibility to the method which despite the increasing number of beamlines suited for PDF studies at large-scale facilities, is still limited. However, data analysis can still be a bottleneck to understand the complex structure of heterogeneous catalysts. In this context, PDF analysis methods are continuously being developed further, allowing to extract either previously inaccessible information from the PDF and/or doing so in a more efficient manner [92–95]. We see an increased use of complex modelling approaches which combine data from multiple characterization techniques and/or ab-initio calculated structures [59,61,70,96,97]. Furthermore, the ongoing progress in automated data processing algorithms is essential to address the challenges of processing big PDF data sets [65,98–101] from in situ/operando and high-throughput experimentation. With further improvements in data analysis and in situ /operando methodology, we believe PDF will play a key role in advancing our knowledge on structure-performance relationship in heterogeneous catalysis, elucidating active phases and deactivation routes.

Outstanding Questions

Can we improve our PDF instrumentation and analysis to ensure that the structure probed in a PDF experiment can be correlated to a certain catalytic performance?

Can new tools such as machine learning approaches or chemometric techniques aid the identification of structural descriptors for catalytic performance from large and complex PDF data sets?

What developments are needed to make PDF an accessible tool for heterogeneous catalysts?

Will the combination of PDF and spectroscopic techniques (such as XAS) under an operando configuration provide a unique kind of experiment that is greater than the sum of its parts?

Considering that catalytic reactions involve largely surface sites, can we design experiments to make PDF more sensitive to the surface structure of the catalyst?

Can PDF be used for single atom catalysts?

Can PDF in combination with theoretical calculations (DFT, metadynamics) improve our knowledge of the structure of small metal and metal oxides clusters (< 1 nm) and their dynamics under reaction conditions?

Thin film-based catalysts are commonly used for (photo)electrocatalysis applications. How can we further improve the signal-to-noise of small sample volumes probed? And can we develop operando PDF of thin films?

When will we see the first in situ ePDF studies?

Can we develop more robust model construction and regression algorithms to solve the structure of nanostructured catalysts? Is a one-fits-all approach realistic?

Which developments can we expect in experimental setups for high throughput PDF?

Acknowledgements

This project has received funding from the European Research Council (ERC) under the European Union's Horizon 2020 research and innovation program grant agreement No. 819573. N.Z. thanks the SINERGIA project (SNF Project No. CRSII2-154448) for financial support. This publication was created as part of NCCR Catalysis, a National Centre of Competence in Research funded by the Swiss National Science Foundation.

References

1 Vogt, C. and Weckhuysen, B.M. (2022) The concept of active site in heterogeneous catalysis. Nat. Rev. Chem. 6, 89–111
2 Filez, M. et al. (2019) Formation and Functioning of Bimetallic Nanocatalysts: The Power of X-ray Probes. Angew. Chem. 131, 13354–13364
3 Qi, G. et al. (2021) Solid-state NMR studies of internuclear correlations for characterizing catalytic materials. Chem. Soc. Rev. 50, 8382–8399
4 Gutmann, T. et al. (2019) Chapter One - Solid-state NMR of nanocrystals. *Annual Reports on NMR Spectroscopy* 97 (Webb, G. A., ed), pp. 1–82, Academic Press
5 Lamberti, C. et al. (2016) XAS Spectroscopy: Related Techniques and Combination with Other Spectroscopic and Scattering Methods. *X-Ray Absorption and X-Ray Emission Spectroscopy* pp. 303–350, John Wiley & Sons, Ltd
6 Holder, C.F. and Schaak, R.E. (2019) Tutorial on Powder X-ray Diffraction for Characterizing Nanoscale Materials. ACS Nano 13, 7359–7365
7 Terban, M.W. and Billinge, S.J.L. (2021) Structural Analysis of Molecular Materials Using the Pair Distribution Function. Chem. Rev. DOI: 10.1021/acs.chemrev.1c00237
8 Billinge, S.J.L. (2019) The rise of the X-ray atomic pair distribution function method: a series of fortunate events. Philos. Trans. Royal Soc. A DOI: 10.1098/rsta.2018.0413
9 Chapman, K.W. and Chupas, P.J. (2013) Pair Distribution Function Analysis of High-Energy X-ray Scattering Data. *In-situ Characterization of Heterogeneous Catalysts* pp. 147–168, John Wiley & Sons, Ltd

10 Zhu, H. et al. (2021) Bridging Structural Inhomogeneity to Functionality: Pair Distribution Function Methods for Functional Materials Development. Adv. Sci. 8, 2003534
11 Christiansen, T.L. et al. (2020) There's no place like real-space: elucidating size-dependent atomic structure of nanomaterials using pair distribution function analysis. Nanoscale Adv. 2, 2234–2254
12 Herbert, J.J. et al. (2016) X-ray spectroscopic and scattering methods applied to the characterisation of cobalt-based Fischer–Tropsch synthesis catalysts. Catal. Sci. Technol. 6, 5773–5791
13 Cusinato, L. et al. (2017) Shape, electronic structure and steric effects of organometallic nanocatalysts: relevant tools to improve the synergy between theory and experiment. Dalton Trans. 46, 378–395
14 Jensen, K.M.Ø. (2021) Characterization of Nanomaterials with Total Scattering and Pair Distribution Function Analysis: Examples from Metal Oxide Nanochemistry. Chimia DOI: 10.2533/chimia.2021.368
15 Takeshi, E. and Billinge, S.J.L. (2012) Chapter 5 - Data Collection Analysis. *Pergamon Materials Series* 16 (Egami, T. and Billinge, S. J. L., eds), pp. 159–257, Pergamon
16 Liu, J. et al. (2018) Large-Scale Synthesis and Comprehensive Structure Study of δ-MnO_2. Inorg. Chem. 57, 6873–6882
17 Juhás, P. et al. (2013) PDFgetX3: a rapid and highly automatable program for processing powder diffraction data into total scattering pair distribution functions. J. Appl. Crystallogr. 46, 560–566
18 Juhás, P. et al. (2018) PDFgetN3: atomic pair distribution functions from neutron powder diffraction data using ad hoc corrections. J. Appl. Crystallogr. 51, 1492–1497
19 Toby, B.H. and Von Dreele, R.B. (2013) GSAS-II: the genesis of a modern open-source all purpose crystallography software package. J. Appl. Crystallogr. 46, 544–549
20 Soper, A.K. (2011) GudrunN and GudrunX: programs for correcting raw neutron and X-ray diffraction data to differential scattering cross section. Rutherford Appleton Laboratory Technical Reports DOI: 10.5286/raltr.2011013
21 Takeshi, E. and Billinge, S.J.L. (2012) Extracting Structural Information from the PDF. *Pergamon Materials Series* 16pp. 259–295, Elsevier
22 Chapman, K.W. and Chupas, P.J. (2013) Pair Distribution Function Analysis of High-Energy X-ray Scattering Data. *In-situ Characterization of Heterogeneous Catalysts* pp. 147–168, John Wiley & Sons, Ltd
23 Farrow, C.L. et al. (2007) PDFfit2 and PDFgui: computer programs for studying nanostructure in crystals. J. Phys.: Condens. Matter 19, 335219
24 Coelho, A.A. (2018) TOPAS and TOPAS-Academic: an optimization program integrating computer algebra and crystallographic objects written in C++. J Appl Cryst 51, 210–218
25 Juhás, P. et al. (2015) Complex modeling: a strategy and software program for combining multiple information sources to solve ill posed structure and nanostructure inverse problems. Acta Crystallogr., Sect. A: Found. Crystallogr. 71, 562–568
26 Proffen, T. and Neder, R.B. (1997) DISCUS: a program for diffuse scattering and defect-structure simulation. J Appl Cryst 30, 171–175
27 Gereben, O. et al. A new version of the RMC++ Reverse Monte Carlo programme, aimed at investigating the structure of covalent glasses.
28 Tucker, M.G. et al. (2007) RMCProfile: reverse Monte Carlo for polycrystalline materials. J. Phys.: Condens. Matter 19, 335218
29 Xie, C. et al. (2020) Defect Chemistry in Heterogeneous Catalysis: Recognition, Understanding, and Utilization. ACS Catal. 10, 11082–11098
30 Devthade, V. et al. (2018) Graphitic Carbon Nitride−γ-Gallium Oxide (GCN-γ-Ga_2O_3) Nanohybrid Photocatalyst for Dinitrogen Fixation and Pollutant Decomposition. ACS Appl. Nano Mater. 1, 5581–5588
31 Castro-Fernández, P. et al. (2021) Propane Dehydrogenation on Ga_2O_3-Based Catalysts: Contrasting Performance with Coordination Environment and Acidity of Surface Sites. ACS Catal.

32 Zhang, X. et al. (2018) Oxygen vacancy modulation of two-dimensional γ-Ga_2O_3 nanosheets as efficient catalysts for photocatalytic hydrogen evolution. Nanoscale 10, 21509–21517
33 Castro-Fernández, P. et al. (2020) Atomic-Scale Insight into the Structure of Metastable γ-Ga_2O_3 Nanocrystals and their Thermally-Driven Transformation to β-Ga_2O_3. J. Phys. Chem. C 124, 20578–20588
34 Luo, S. et al. (2021) New Insights into the Bulk and Surface Defect Structures of Ceria Nanocrystals from Neutron Scattering Study. Chem. Mater. 33, 3959–3970
35 Ramanathan, A. et al. (2021) In-Plane Cation Ordering and Sodium Displacements in Layered Honeycomb Oxides with Tetravalent Lanthanides: Na_2LnO_3 (Ln = Ce, Pr, and Tb). Inorg. Chem. 60, 1398–1410
36 Batchellor, A.S. et al. (2017) Domain Structures of Ni and NiFe (Oxy)Hydroxide Oxygen-Evolution Catalysts from X-ray Pair Distribution Function Analysis. J. Phys. Chem. C 121, 25421–25429
37 Pakharukova, V.P. et al. (2021) Application of pair distribution function analysis to structural investigation of alumina supported MoS_2 catalysts. Colloids Interface Sci. Commun. 43, 100454
38 Wada, T. et al. (2020) Revisiting the identity of δ-$MgCl_2$: Part I. Structural disorder studied by synchrotron X-ray total scattering. Journal of Catalysis 385, 76–86
39 Wada, T. et al. (2020) Structural Disorder of Mechanically Activated δ-$MgCl_2$ Studied by Synchrotron X-ray Total Scattering and Vibrational Spectroscopy. Catalysts 10, 1089
40 Shang, H. et al. (2018) N-doped graphdiyne for high-performance electrochemical electrodes. Nano Energy 44, 144–154
41 Sun, J. et al. (2017) Pressure-Induced Polymerization of Acetylene: Structure-Directed Stereoselectivity and a Possible Route to Graphane. Angew. Chem., Int. Ed. 56, 6553–6557
42 Metz, P.C. et al. (2018) Differential evolution and Markov chain Monte Carlo analyses of layer disorder in nanosheet ensembles using total scattering. J. Appl. Crystallogr. 51, 1437–1444
43 Tsunekawa, S. et al. (2020) Operando Observations of a Manganese Oxide Electrocatalyst for Water Oxidation Using Hard/Tender/Soft X-ray Absorption Spectroscopy. J. Phys. Chem. C 124, 23611–23618
44 Cao, C. et al. (2017) Graphene-like δ-MnO_2 decorated with ultrafine CeO_2 as a highly efficient catalyst for long-life lithium–oxygen batteries. J. Mater. Chem. A 5, 6747–6755
45 Willinger, E. et al. (2017) Identifying Key Structural Features of IrO_x Water Splitting Catalysts. J. Am. Chem. Soc. 139, 12093–12101
46 Tominaka, S. et al. (2017) Noncrystalline Titanium Oxide Catalysts for Electrochemical Oxygen Reduction Reactions. ACS Omega 2, 5209–5214
47 Donakowski, M.D. et al. (2018) Trapping a Ru_2O_3 Corundum-like Structure at Ultrathin, Disordered RuO_2 Nanoskins Expressed in 3D. J. Phys. Chem. C 122, 28895–28900
48 Kwon, G. et al. (2018) Resolution of Electronic and Structural Factors Underlying Oxygen-Evolving Performance in Amorphous Cobalt Oxide Catalysts. J. Am. Chem. Soc. 140, 10710–10720
49 Kwon, G. et al. (2021) Experimental Verification of Ir 5d Orbital States and Atomic Structures in Highly Active Amorphous Iridium Oxide Catalysts. ACS Catal. 11, 10084–10094
50 Şahin, E.O. et al. (2021) In situ total scattering experiments of nucleation and crystallisation of tantalum-based oxides: from highly dilute solutions via cluster formation to nanoparticles. Nanoscale 13, 150–162
51 Souza Junior, J.B. et al. (2021) Pair Distribution Function Obtained from Electron Diffraction: An Advanced Real-Space Structural Characterization Tool. Matter 4, 441–460
52 Pakharukova, V.P. et al. (2021) Investigation of the Structure and Interface Features of Ni/$Ce_{1-x}Zr_xO_2$ Catalysts for CO and CO_2 Methanation. J. Phys. Chem. C 125, 20538–20550
53 Derevyannikova, E.A. et al. (2019) Structural Insight into Strong Pt–CeO_2 Interaction: From Single Pt Atoms to PtO_x Clusters. J. Phys. Chem. C 123, 1320–1334
54 Senecal, P. et al. (2017) Real-Time Scattering-Contrast Imaging of a Supported Cobalt-Based Catalyst Body during Activation and Fischer–Tropsch Synthesis Revealing Spatial Dependence of Particle Size and Phase on Catalytic Properties. ACS Catal. 7, 2284–2293

55 Daoura, O. et al. (2021) One-pot prepared mesoporous silica SBA-15-like monoliths with embedded Ni particles as selective and stable catalysts for methane dry reforming. Appl. Catal., B 280, 119417
56 Ortatatlı, Ş. et al. (2018) Monitoring the formation of PtNi nanoalloys supported on hollow graphitic spheres using in situ pair distribution function analysis. Phys. Chem. Chem. Phys. 20, 8466–8474
57 Prinz, N. et al. (2020) Hard X-ray-based techniques for structural investigations of CO_2 methanation catalysts prepared by MOF decomposition. Nanoscale 12, 15800–15813
58 Kong, Z. et al. (2020) Origin of High Activity and Durability of Twisty Nanowire Alloy Catalysts under Oxygen Reduction and Fuel Cell Operating Conditions. J. Am. Chem. Soc. 142, 1287–1299
59 Nguyen, A.I. et al. (2019) Stabilization of reactive Co_4O_4 cubane oxygen-evolution catalysts within porous frameworks. PNAS 116, 11630–11639
60 Benseghir, Y. et al. (2020) Co-immobilization of a Rh Catalyst and a Keggin Polyoxometalate in the UiO-67 Zr-Based Metal–Organic Framework: In Depth Structural Characterization and Photocatalytic Properties for CO_2 Reduction. J. Am. Chem. Soc. 142, 9428–9438
61 Simons, M.C. et al. (2019) Structure, Dynamics, and Reactivity for Light Alkane Oxidation of Fe(II) Sites Situated in the Nodes of a Metal–Organic Framework. J. Am. Chem. Soc. 141, 18142–18151
62 Knorpp, A.J. et al. (2021) Paired Copper Monomers in Zeolite Omega: The Active Site for Methane-to-Methanol Conversion. Angew. Chem. 133, 5918–5922
63 Usui, T. et al. (2019) Identifying the Factors Governing the Early-Stage Degradation of Cu-Chabazite Zeolite for NH_3-SCR. ACS Omega 4, 3653–3659
64 Iida, T. et al. (2018) Concerted Bimetallic Nanocluster Synthesis and Encapsulation via Induced Zeolite Framework Demetallation for Shape and Substrate Selective Heterogeneous Catalysis. Angew. Chem., Int. Ed. 57, 6454–6458
65 Lindahl Christiansen, T. et al. (2020) Structure analysis of supported disordered molybdenum oxides using pair distribution function analysis and automated cluster modelling. J. Appl. Crystallogr. 53, 148–158
66 Liu, J. et al. (2019) Metal–Organic-Framework-Supported and -Isolated Ceria Clusters with Mixed Oxidation States. ACS Appl. Mater. Interfaces 11, 47822–47829
67 Iida, T. et al. (2017) Encapsulation of Molybdenum Carbide Nanoclusters inside Zeolite Micropores Enables Synergistic Bifunctional Catalysis for Anisole Hydrodeoxygenation. ACS Catal. 7, 8147–8151
68 Platero-Prats, A.E. et al. (2017) Addressing the characterisation challenge to understand catalysis in MOFs: the case of nanoscale Cu supported in NU-1000. Faraday Discuss. 201, 337–350
69 Kalantzopoulos, G.N. et al. (2018) In Situ Flow MAS NMR Spectroscopy and Synchrotron PDF Analyses of the Local Response of the Brønsted Acidic Site in SAPO-34 during Hydration at Elevated Temperatures. ChemPhysChem 19, 519–528
70 O'Nolan, D. et al. (2021) A multimodal analytical toolkit to resolve correlated reaction pathways: the case of nanoparticle formation in zeolites. Chem. Sci. 12, 13836–13847
71 Louwen, J.N. et al. (2020) Understanding the Activation of ZSM-5 by Phosphorus: Localizing Phosphate Groups in the Pores of Phosphate-Stabilized ZSM-5. Chem. Mater. 32, 9390–9403
72 Stassin, T. et al. (2020) Solvent-Free Powder Synthesis and MOF-CVD Thin Films of the Large-Pore Metal–Organic Framework MAF-6. Chem. Mater. 32, 1784–1793
73 Chen, Z. et al. (2021) Mechanistic Insights into Nanoparticle Formation from Bimetallic Metal–Organic Frameworks. J. Am. Chem. Soc. 143, 8976–8980
74 Zhou, Y. et al. (2021) The synthesis of SAPO-34 zeolite for an improved MTO performance: tuning the particle size and an insight into the formation mechanism. Inorg. Chem. Front. 8, 2315–2322
75 Kwon, G. et al. (2019) Microfluidic electrochemical cell for in situ structural characterization of amorphous thin-film catalysts using high-energy X-ray scattering. J. Synchrotron Rad. 26, 1600–1611

76 Wu, Z.-P. et al. (2021) Alloying–realloying enabled high durability for Pt–Pd-3d-transition metal nanoparticle fuel cell catalysts. Nat. Commun. 12, 859
77 Diaz-Lopez, M. et al. (2020) Fast operando X-ray pair distribution function using the DRIX electrochemical cell. J. Synchrotron Rad. 27, 1190–1199
78 Shi, X. et al. (2021) Dynamics of Heterogeneous Catalytic Processes at Operando Conditions. JACS Au DOI: 10.1021/jacsau.1c00355
79 Petkov, V. et al. (2018) Evolution of Active Sites in Pt-Based Nanoalloy Catalysts for the Oxidation of Carbonaceous Species by Combined in Situ Infrared Spectroscopy and Total X-ray Scattering. ACS Appl. Mater. Interfaces 10, 10870–10881
80 Petkov, V. et al. (2018) Nanoalloy catalysts inside fuel cells: An atomic-level perspective on the functionality by combined in operando x-ray spectroscopy and total scattering. Nano Energy 49, 209–220
81 van Beek, W. et al. (2019) MS42-P04 | SNBL'S BM31 AT ESRF BEYOND 2020 - COMBINED XRD-PDF-XAS. Acta Crystallogr., Sect. E: Struct. Rep. Online A75, e677
82 Rantanen, J. et al. (2019) The atomic local ordering of SBA-15 studied with pair distribution function analysis, and its relationship to porous structure and thermal stability. Acta Mater. 175, 341–347
83 Thomae, S.L.J. et al. (2019) Pushing data quality for laboratory pair distribution function experiments. Rev. Sci. Instrum. 90, 043905
84 Teck, M. et al. (2017) Structural and spectroscopic comparison between polycrystalline, nanocrystalline and quantum dot visible light photo-catalyst Bi_2WO_6. J. Solid State Chem. 254, 82–89
85 Takimoto, D. et al. (2019) Conductive Nanosized Magnéli-Phase Ti_4O_7 with a Core@Shell Structure. Inorg. Chem. 58, 7062–7068
86 Corrêa, L.M. et al. (2021) Quantitative Structural Analysis of AuAg Nanoparticles Using a Pair Distribution Function Based on Precession Electron Diffraction: Implications for Catalysis. ACS Appl. Nano Mater. 4, 12541–12551
87 Ponce, A. et al. (2021) Advances in the electron diffraction characterization of atomic clusters and nanoparticles. Nanoscale Adv. 3, 311–325
88 Gorelik, T.E. et al. (2019) Towards quantitative treatment of electron pair distribution function. Acta Crystallogr., Sect. B: Struct. Sci. 75, 532–549
89 Hoque, M.M. et al. (2019) Structural Analysis of Ligand-Protected Smaller Metallic Nanocrystals by Atomic Pair Distribution Function under Precession Electron Diffraction. J. Phys. Chem. C 123, 19894–19902
90 Ngo, D.-T. et al. (2018) Local Structure and Chemistry of C-Doped ZnO@C Core–Shell Nanostructures with Room-Temperature Ferromagnetism. Adv. Funct. Mater. 28, 1704567
91 Martin, A.V. et al. (2020) Detection of Ring and Adatom Defects in Activated Disordered Carbon via Fluctuation Nanobeam Electron Diffraction. Small 16, 2000828
92 Gamez-Mendoza, L. et al. (2017) Modelling and validation of particle size distributions of supported nanoparticles using the pair distribution function technique. J. Appl. Crystallogr. 50, 741–748
93 Bird, T.A. et al. (2021) Symmetry-adapted pair distribution function analysis (SAPA): a novel approach to evaluating lattice dynamics and local distortions from total scattering data. J. Appl. Crystallogr. 54, 1514–1520
94 Yang, L. et al. (2021) A cloud platform for atomic pair distribution function analysis: PDFitc. Acta Crystallogr., Sect. A: Found. Crystallogr. 77, 2–6
95 Geddes, H.S. et al. (2021) Extracting interface correlations from the pair distribution function of composite materials. Nanoscale 13, 13220–13224
96 Koch, R.J. et al. (2020) Complex modeling for the quantification of nanoscale disorder using genetic algorithms, density functional theory and line-profile analysis. J. Appl. Crystallogr. 53, 1087–1100

97 Wu, Z.-P. et al. (2018) Revealing the Role of Phase Structures of Bimetallic Nanocatalysts in the Oxygen Reduction Reaction. ACS Catal. 8, 11302–11313
98 Yang, L. et al. (2020) Structure-mining: screening structure models by automated fitting to the atomic pair distribution function over large numbers of models. Acta Crystallogr., Sect. A: Found. Crystallogr. 76, 395–409
99 Gu, R. et al. (2019) Algorithm for distance list extraction from pair distribution functions. Acta Crystallogr., Sect. A: Found. Crystallogr. 75, 658–668
100 Olds, D. et al. (2017) Combinatorial appraisal of transition states for in situ pair distribution function analysis. J. Appl. Crystallogr. 50, 1744–1753
101 Liu, C.-H. et al. (2021) Validation of non-negative matrix factorization for rapid assessment of large sets of atomic pair distribution function data. J. Appl. Crystallogr. 54, 768–775

Glossary

Atomic form factor, f(Q): Is a measure of the scattering amplitude of a wave by an isolated atom.

Coherent scattering: A scattering process in which the energy of the incident and outgoing waves do not change. It is also called elastic scattering.

Crystal defects: All deviations from the ideal crystal (see unit cell) are referred to as crystal defects. Some examples are substitution defects, vacancies, or stacking faults.

Diffuse scattering: Elastic and inelastic diffuse scattering together with the Bragg peaks make up the total scattering intensity. Diffuse scattering contains information on the static and dynamic (due to the movement of atoms) local structure. It extends over a wide range of Q and is weaker than the coherent scattering; therefore, it is more challenging to measure than Bragg peaks.

Frenkel defects: A type of crystal defect where an atom has "wandered" to a place in between other atoms (interstitial site). A Frenkel-type oxygen vacancy thus describes an oxygen atom which occupies an interstitial site in the crystal lattice and leaves behind a vacant site.

In situ: In an in situ study, a material property (such as its structure, surface chemistry or composition) is probed over time under specific conditions (e.g. elevated temperature, gas or liquid flow).

Operando: Refers to a specific case of an in situ study where the catalyst is exposed to reaction conditions while the products and reactants are simultaneously analysed and quantified.

Momentum transfer vector, Q: Defined as the difference between the incident wave vector $\mathbf{k}_0$ and the scattered wave vector $\mathbf{k}_1$ in a scattering experiment: $\mathbf{Q} = \mathbf{k}_0 - \mathbf{k}_1$. The magnitude of **Q** is defined in equation [1].

Rw: Weighted R-value to quantify goodness of the PDF fit. A perfect fit between a model structure and the acquired data leads to Rw = 0.

Stacking fault: Is a type of planar crystal defect describing the non-ideal stacking of layers of atoms. Turbostratic stacking faults are a type of stacking fault where the layers are randomly rotated or translated relative to each other.

Structure function, S(Q): Is the equivalent of the PDF in reciprocal space. It represents the normalized, coherently scattered intensity from the sample.

Supercell: As mentioned below, unit cells fully describe the structure of perfect crystals. When defects are introduced into the crystal structure, the symmetry of the crystal is reduced. The supercell approach involves the merging of multiple unit cells into a larger supercell, containing a certain number of defects. Repeating of the supercell in space describes better the structure of a disordered crystal compared to the unit cell.

Unit cell: An ideal crystal can be described by a single volume called unit cell, containing all the unique atomic positions of the structure. By translation of the unit cell in 3D space, a crystal of the desired size can be generated.